Biomedicine & Pharmacotherapy 171 (2024) 116104

Contents lists available at ScienceDirect

Biomedicine & Pharmacotherapy

journal homepage: www.elsevier.com/locate/biopha

Au@16-pH-16/miR-21 mimic nanosystem: An efficient treatment for obesity through browning and thermogenesis induction

Said Lhamyani [a,b,c,1], Adriana-Mariel Gentile [a,b,1], María Mengual-Mesa [a,d,1], Elia Grueso [e], Rosa M. Giráldez-Pérez [f], José Carlos Fernandez-Garcia [a,b,c], Antonio Vega-Rioja [g,n], Mercedes Clemente-Postigo [a,c,h,i], John R. Pearson [j], Isabel González-Mariscal [a,m], Gabriel Olveira [a,b,k,l], Francisco-Javier Bermudez-Silva [a,b,k], Rajaa El Bekay [a,b,c,*]

[a] Instituto de Investigación Biomédica de Málaga y Plataforma en Nanomedicina-IBIMA Plataforma BIONAND, 29580 Malaga, Spain
[b] Clinical Unit of Endocrinology and Nutrition, University Regional Hospital of Malaga, 29009 Malaga, Spain
[c] Obesity and Nutrition CIBER (CIBERobn), Instituto de Salud Carlos III, Madrid, Spain
[d] Universidad de Málaga. Andalucía Tech, Faculty of Health Sciences, Department of Systems and Automation Engineering, Malaga, Spain
[e] Departamento de Física Química, Facultad de Farmacia, Universidad de Sevilla, Sevilla, Spain
[f] Departamento de Biología Celular, Fisiología e Inmunología, Universidad de Córdoba, Córdoba, Spain
[g] Laboratorio de Inmunología y Alergia-FISEVI, UGC de Alergología. Hospital Universitario Virgen Macarena, Sevilla, Spain
[h] Department of Endocrinology and Nutrition, Virgen de la Victoria University Hospital, Malaga, Spain
[i] Department of Cell Biology, Genetics, and Physiology, Faculty of Science, University of Malaga, Malaga, Spain
[j] Instituto de Biomedicina de Sevilla (IBiS), Seville, Spain
[k] The Spanish Biomedical Research Centre in Diabetes and Associated Metabolic Disorders (CIBERDEM), Madrid, Spain
[l] Departamento de Medicina y Cirugía, Universidad de Málaga, Málaga, Spain
[m] Inserm UMR1190, CHU de Lille, Universite de Lille, Institute Pasteur de Lille, Lille, France
[n] Departamento de Medicina. Facultad de Medicina. Universidad de Sevilla, Sevilla, Spain

ARTICLE INFO

Keywords:
MiRNA
Gold Nanoparticles
Gemini surfactant
Obesity
Adipose tissue
Browning
Thermogenesis

ABSTRACT

Despite the abundance of registered clinical trials worldwide, the availability of effective drugs for obesity treatment is limited due to their associated side effects. Thus, there is growing interest in therapies that stimulate energy expenditure in white adipose tissue. Recently, we demonstrated that the delivery of a miR-21 mimic using JetPEI effectively inhibits weight gain in an obese mouse model by promoting metabolism, browning, and thermogenesis, suggesting the potential of miR-21 mimic as a treatment for obesity. Despite these promising results, the implementation of more advanced delivery system techniques for miR-21 mimic would greatly enhance the advancement of safe and efficient treatment approaches for individuals with obesity in the future. Our objective is to explore whether a new delivery system based on gold nanoparticles and Gemini surfactants (Au@16-ph-16) can replicate the favorable effects of the miR-21 mimic on weight gain, browning, and thermogenesis. We found that dosages as low as 0.2 μg miR-21 mimic /animal significantly inhibited weight gain and induced browning and thermogenic parameters. This was evidenced by the upregulation of specific genes and proteins associated with these processes, as well as the biogenesis of beige adipocytes and mitochondria. Significant increases in miR-21 levels were observed in adipose tissue but not in other tissue types. Our data indicates that Au@16-ph-16 could serve as an effective delivery system for miRNA mimics, suggesting its potential suitability for the development of future clinical treatments against obesity.

1. Introduction

Obesity is a widespread epidemic disease and is considered one of the major health problems of modern societies. It is tightly associated with multiple serious comorbidities, such as type 2 diabetes (T2D), insulin resistance (IR), cardiovascular diseases, mental health, and cancers,

* Correspondence to: IBIMA-Plataforma Bionand, Hospital Regional Universitario de Málaga, Plaza Hospital Civil s/n. Pabellón 5, Sótano, Málaga, Spain.
E-mail address: elbekay@gmail.com (R. El Bekay).
[1] These authors share first authorship

https://doi.org/10.1016/j.biopha.2023.116104
Received 25 April 2023; Received in revised form 21 December 2023; Accepted 26 December 2023
Available online 9 January 2024

which decrease life expectancy [1,2].

Different pharmacological approaches have been proposed as an alternative or complement to diet, exercise, and bariatric surgery. However, the available anti-obesity treatments are still limited due to their side effects or modest and/or unsustainable effects [3–5].

Therapies targeting thermogenic brown adipose tissue (BAT) and affecting energy expenditure have garnered great interest since 2009, when it was first reported that active BAT is present in adult humans located in the supraclavicular, neck paravertebral, and suprarenal areas, using positron emission tomography-computed tomography (PET-CT) [6,7]. BAT plays a vital role in regulating energy balance and homeostasis through its thermogenic activity and its role as an endocrine organ. As a result, it has been proposed as a target to enhance weight loss and insulin sensitivity [8,9]. Furthermore, in response to specific stimuli, white adipose tissue (WAT) can be transformed into beige adipose tissue (AT) through a process called browning. Beige AT shares characteristics with BAT, such as uncoupling protein 1 (UCP1) and TMEM26 expression, and multilocular adipocytes with high mitochondrial content [8,10]. This transformation may play a crucial role in energy consumption and could protect against obesity [11–14].

MicroRNAs (miRNAs) are small, single-stranded non-coding RNAs (~21–25 nucleotides) that regulate gene expression at the post-transcriptional level and participate in biological processes such as cell differentiation, apoptosis, angiogenesis, and adipogenesis [15–17]. In recent years, there has been growing interest in the pivotal roles that miRNAs may play in obesity through the regulation of WAT, beige AT, and BAT differentiation and function [18–21]. In this regard, several studies have shown the involvement of miR-21 in adipogenesis and obesity [19,22,23]. miR-21 has been found to be overexpressed in WAT from obese subjects compared to normoweight individuals [24] and to enhance adipogenic differentiation through the modulation of transforming growth factor (TGF)-β signaling [25,26].

miRNA replacement therapy, also known as the use of miRNA mimics, has gained interest in recent years [27]. These synthetic miRNAs mimic the function of endogenous miRNAs and bind directly to the RNA-induced silencing complex (RISC) to interact with their respective target mRNAs and produce an effect on the expression of genes similar to that driven by the original miRNA [27]. Recently, our group described that a synthetic miR-21 mimic blocks obesity in mice through metabolic enhancement, WAT browning, and BAT thermogenic re-programming [19]. These novel results suggest that miR-21 mimic-based therapy may provide a new opportunity to manage obesity. Once the therapeutic potential of miR-21 mimics for treating obesity is established, the next challenge is to identify an efficient method of targeted administration with low toxicity, facilitating the competent delivery of miR-21 directly to AT. Historically, the dominant strategy to achieve drug accumulation at specific tissue sites involves further engineering drug delivery vehicles to feature a targeting ligand that recognizes a tissue-specific target molecule, thereby minimizing off-target accumulation [28]. In our case, despite achieving positive effects with JetPEI as a delivery system for the miR21 mimic and observing no adverse effects in the animal model used in the previous study [19], designing a therapy specifically targeted to AT with this vehicle may not be possible or would require intricate engineering. Currently, numerous ongoing clinical trials are investigating nanoparticle-based drug delivery systems for administering anticancer agents, antibiotics, anti-inflammatory drugs, and more, with the goal of achieving improved targeted therapy while minimizing side effects [29,30]. Inorganic materials, such as gold, iron, and silica, have been employed to synthesize nanostructured materials for various drug delivery and imaging applications. The precise formulation of these inorganic nanoparticles (NPs) enables the engineering of a wide variety of sizes, structures, and geometries. Among these inorganic NPs, gold nanoparticles (AuNPs) have been extensively studied. They can take various forms, including nanospheres, nanorods, nanostars, nanoshells, and nanocages [31]. Functionalized AuNPs exhibit excellent biocompatibility, low cytotoxicity, and a high surface-to-volume ratio [32]. Their size and surface modifications play a crucial role in biodistribution, allowing targeted accumulation in specific organs while evading the reticuloendothelial system [31]. Additionally, gold nanoparticles can form robust associations with cationic gemini surfactants, serving as valuable carriers due to their low toxicity, biodegradability, and efficient compaction of RNA molecules [33–35].

Recently, our group has developed a nanosystem named Au@ 16-ph-16/miR-21 mimic, comprising gold nanoparticles, gemini surfactant, and synthetic miRNA mimic. This nanosystem stands out due to its gemini surfactant with lipophilic characteristics, facilitated by the presence of two hydrophobic (lipophilic) tails in its molecular structure [36,37]. Compared to traditional single-tailed surfactants, this design grants the nanosystem enhanced lipophilic properties, making it highly effective in solubilizing lipophilic compounds [33]. Furthermore, this nanosystem exhibits excellent biocompatibility and non-toxicity, ensuring its safety for potential therapeutic use. Notably, it also demonstrates significant anti-microbial activities [33], adding to its versatility and potential applications. Given these outstanding characteristics, our nanosystem holds great promise as a potential therapeutic option for addressing obesity and other related conditions. The combination of gold nanoparticles, gemini surfactant, and synthetic miRNA mimic opens new possibilities in targeted drug delivery and personalized medicine approaches.

The aim of this study is to investigate whether the implementation of Au@ 16-ph-16 nanocarrier as a delivery system could preserve the beneficial effects of the miR-21 mimic on weight gain, browning, and thermogenesis in the animal model of obesity and to optimize the dosage of the miR-21 mimic utilized for better outcomes.

2. Materials and methods

2.1. Mice and diet-induced obesity

C57BL/6 J mice (The Jackson Laboratory) were used to obtain obese phenotypes after 8 weeks high fat diet (HFD 45% kcal, D12451; Research Diets, New Brunswick, NJ, USA). As we previously described, mice were housed individually in adequate temperature and humidity conditions and with free access to pelleted chow. Body weight was monitored twice a week [19].

All experimental protocols and procedures were approved by the University of Malaga Ethics Committee (authorization no. CEUMA N. º 91–2021-A) and were in accordance with the European Union recommendations (2010/63/EU). G*Power software was used to determine the suitable number of animals for this study with $\alpha = 0.05$ and $1\text{-}\beta = 0.95$.

2.2. Synthesis of Au@16-ph-16 precursor gold nanoparticles

Gemini surfactants functionalized with gold nanoparticles were prepared by direct synthesis based on hydrogen tetrachloroaurate (III) hydrate (HAuCl4·4H2O) in-situ reduction, adding NaBH4 as reductor agent and appropriate Gemini surfactant as stabilizing agent. It is well known that the ratio of AuNPs/Gemini surfactant concentration and the surfactant critical micelle concentration (cmc) value is crucial for parameter stability and nanosystem size optimization. The relation between [Gemini surfactant]/cmc was equal to 5, establishing a lower and an upper limit of 1 and 20, respectively, as a necessary condition for obtaining monodisperse and stable nanosystems. 390 μl of HAuCl4 23 mM aqueous solution was added to 30 mL of 16-ph-16 Gemini surfactant $4{\cdot}10^{-5}$ M aqueous solutions and stirred vigorously. The yellow solutions obtained were stirred for 5 min in the absence of light. 100 μl of a freshly prepared 0.4 M NaBH4 aqueous solution was then added drop by drop to the previously prepared solutions and the mixture stirred moderately for 15 min in darkness, acquiring a reddish color. As a result, a $5.6{\cdot}10^{-8}$ M aqueous solution of Au@ 16-ph-16 gold nanoparticles, was obtained [33].

2.3. Synthesis of Au@16-ph-16/miR-21 mimic gold nanoparticles

Au@16-ph-16/miR-21 mimic was synthesized as previously described [33]. Briefly, the nanosystem synthesis was stabilized with Gemini surfactants and then binding with miR-21 was carried out using an excess of polymer. Different nanosystem formulations were explored using a fixed CAu@m-s-m = $5.6{\cdot}10^{-9}$ M for Au@16-ph-16 and variable CmiR-21 = $4.5{\cdot}10^{-8}$ M, $6.0{\cdot}10^{-8}$ M. As a result, different R = CAu@m-s-m/CmiR-21 ratios were explored in each system: R = 0.124, 0.093 and 0.063 for Au@16-ph-16/miR-21 mimic. In this way, stable Au@16-ph-16/miR-21 mimic complexes were obtained after 30 min of continuous agitation at the room temperature, and subsequent conditioning of the samples obtained at a temperature of 277.0 K for 24 h. A moderate change in the solution color to a slightly purple tone was indicative of complex stabilization (Fig. 1A).

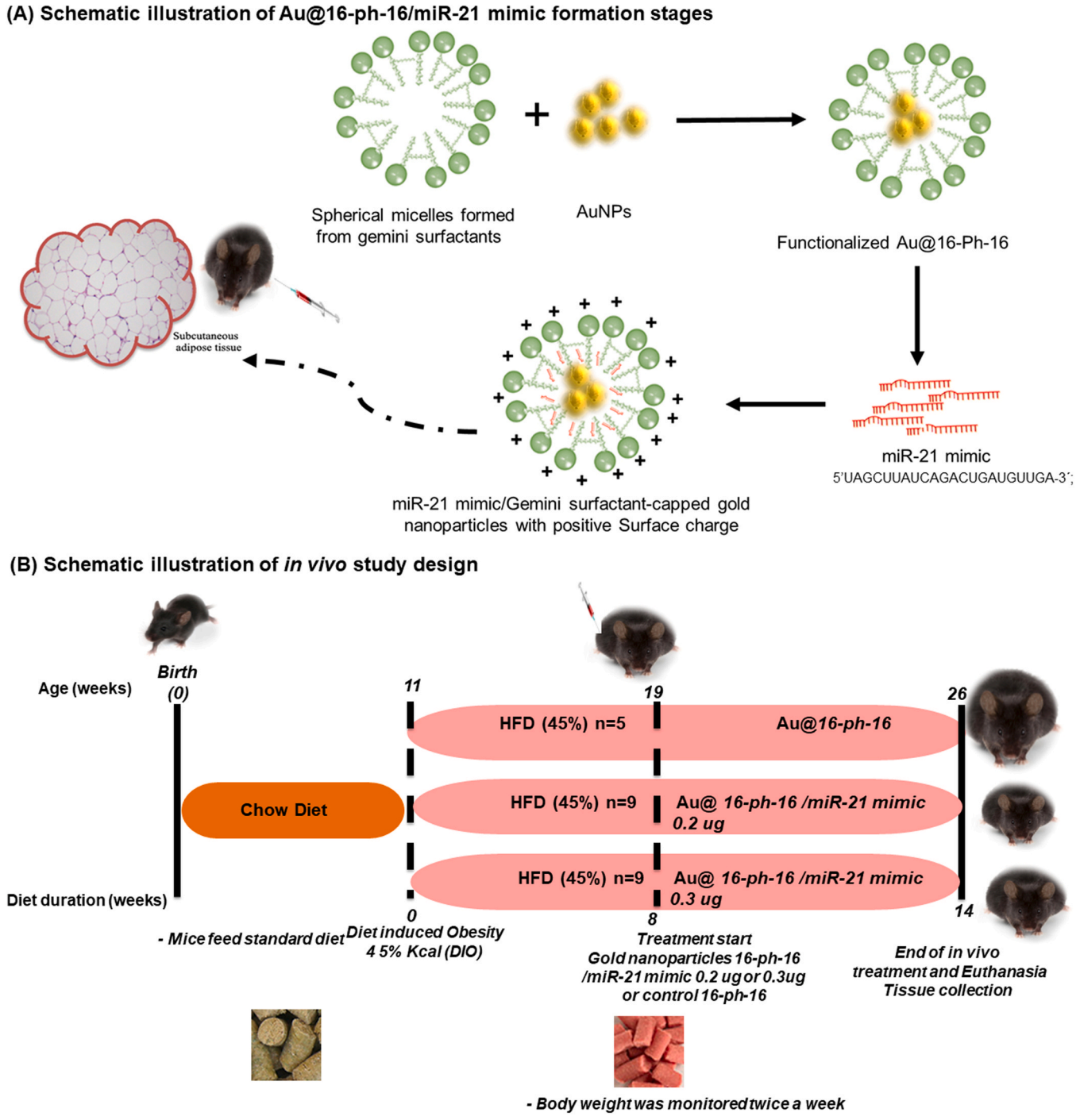

Fig. 1. Schematic illustration of Au@16-ph-16/miR-21 mimic formation stages and *in vivo* study design. (A) A functional nanosystem consisting of miR-21 mimic and gold nanoparticles was synthesized in three steps. First, the gemini surfactant was synthesized, followed by functionalization of gold nanoparticles with the gemini surfactant. Finally, the nanosystem was coated with miR-21 polymer for use in mice treatment. (B) Eleven-week-old C57BL/6 J mice were fed a 45% high-fat diet (HFD) for eight weeks to induce an obese phenotype. The obese mice were then divided into three treatment groups: 0.2 μg (n = 9), 0.3 μg (n = 9) of Au@16-ph-16/miR-21 mimic, and a control group treated with Au@16-ph-16 (n = 5). Mice were treated and weighed twice a week throughout the study.

2.4. In vivo Au@16-ph-16/miR-21 mimic nanosystem mice treatment

After 8 weeks of HFD feeding, obese mice were treated three times a week during 6 weeks by subcutaneous injections in inguinal pad, and according to the injected treatment were separated into three groups: (1) A group treated with 200 μl Au@16-ph-16/ miR-21 mimic 0.2 μg (n = 9), (2) a group treated with 200 μl Au@ 16-ph-16/miR-21 mimic 0.3 μg (n = 9) (5´-UAGCUUAUCAGACUGAUGUUGA-3´; CONmiR mimic *in vivo*, M-00303–0100; Riboxx), and (3) a group treated with the corresponding control treated with 200 μl Au@ 16-ph-16 (n = 5). *In vivo* miRNA mimic (CONmiR; Riboxx, Meissner Straße 191, 01445 Radebeul Germany) is a hybrid miRNA composed of a mature miRNA sequence (guide strand) and its complementary sequence (passenger strand) furnished with RNAi-cap technology, which improves the stability of mimic miRNA and offers optimal and effective gene silencing by facilitating the incorporation of guide strand to the RISC complex [19,38]. Body weight was monitored twice a week. Cumulative weight gain and area under curve (AUC) were calculated using the last weight before treatment for each mouse as a basal point (0 g). At the end of the experiment, mice were sacrificed by cervical dislocation. Plasma and AT depots, BAT, interescapular WAT (intWAT), inguinal WAT (ingWAT) and visceral AT (VAT), heart, spleen, liver, kidney, and brain were isolated, flash frozen in liquid nitrogen and then stored at − 80 °C (Fig. 1**B**).

2.5. GTT measurement

In the *in vivo* study, GTT was assessed in the mice groups at the end of the treatment. Mice were injected intraperitoneally with 2 g/kg of D-glucose (Sigma- Aldrich, St. Louis, MO, USA) after 10–12 h of fasting and blood glucose was measured at 0 (basal), 15, 30, 45, 60, and 120 min from the tail vein using a glucometer (Accu-Chek; Roche Diagnostics, Barcelona, Spain).

2.6. miRNA isolation from adipose tissue and quantitative real-time PCR (qRT-PCR)

miRNA was extracted from ingWAT, VAT, BAT, kidney, heart, spleen, liver, and brain (80–100 mg) using miRvana miRNA isolation kit (AM1561; Ambion, Spain) according to the manufacturer's recommendations. Total RNA was quantified using a Nanodrop ND-2000 (Thermo Fisher Scientific, USA). Reverse transcription (RT) reaction was carried out using Taqman microRNA reverse transcription (4366597) following the manufactureŕs protocol and using miRNA specific primers, namely, hsa-miR-21 (000397) or miRNA control assay, snoRNA-142 (001231). qRT-PCR was performed using Agilent Mx3005P qPCR system and the above indicated specific Taqman probes in a total volume of 20 μl. Cycle threshold (Ct) was determined during amplification and signals was normalized using snoRNA-142 as reference gene [19]. Expression levels were calculated using the formula $2^{-\Delta ct}$, ($\Delta ct = ct_{miR\text{-}21} - ct_{snoRNA\text{-}142}$).

2.7. Total RNA isolation from adipose tissue and quantitative real-time PCR (qRT-PCR)

Total RNA was isolated from 100 mg of ATs using Qiazol RNeasy Lipid Tissue mini kit (QIAGEN, Valencia, CA, USA) according to manufactureŕs protocol. RT reaction was performed using, reverse transcriptase 20 U/mL, (03531287001; Roche), RNase inhibitor (03335399001; Roche) and desoxynucleoside triphosphate (11969064001; Roche). Then, qRT-PCR reactions were performed using 10 ng of cDNA and specific probes. Next, Ct of each gene was determined during amplification and then, specific signals were normalized using *Tbp* as a reference (Mm 00446973). Expression levels were calculated using the formula $2^{-\Delta ct}$. The Taqman genes used in this study were: *Vegf-A* (Mm 00437306-m1), *Ucp1* (Mm 01244861), *Tmem26* (Mm 01173641-m1), *Pgc-1a* (Mm 01208835), *Prdm16* (Mm00556-m1), *Cidea* (Mm00432554-m1), *Ppar-γ* (Mm 00440940-m1), *P53* (Mm01731290-g1), *Tgfβ*1 (Mm01178820-m1), *Fgf21* (Mm 00840165-g1) and *Sirt1* (Mm01168521-m1).

2.8. Mitochondrial DNA analysis

To evaluate the *in vivo* effect of miR-21 mimic treatment on mitochondrial content, cytochrome c oxidase subunit 1 expression (*Cox1*) was analyzed in ingWAT. Total DNA was isolated from ingWAT using the DNeasy Blood and Tissue Kit (QIAGEN, Valencia, CA, USA) according to the manufactureŕs protocol. Then, multiplex qRT-PCR reaction was carried out using specific Taqman probes [*Cox1* (Mm 04225243); *GADPH* (4352339E)]160 ng of DNA and reference dye. The relative mitochondrial DNA (mtDNA) content was calculated using the formula mtDNA= $2^{-(ct\ COX1\text{-}ct\ GADPH)}$, being *Cox1* the mitochondrial factor and *Gadph* the nuclear factor (nDNA).

2.9. Histochemical study and immunofluorescence

AT biopsies were fixed in 4% buffer formaldehyde for 48 h, dehydrated in graded ethanol and embedded in paraffin using Spin Tissue Processor (TP) STP120 and paraffin-embedding center (EG1150H; Leica, Nussloch, Germany). Serial paraffin Section (5μm thick) of each AT sample were cut with a microtome and then adequately processed for histochemical and immunofluorescence analysis.

Next, AT sections were deparaffinized, hydrated in graded ethanol and stained first with Harris Hematoxylin (H&H) nuclear staining for 2 min, followed by cytoplasmic staining using a mixture of eosin and 0.2% glacial acetic for 40 s. Slides were dehydrated by incubation in increasing ethanol concentrations. All samples were photographed using an Olympus BX61 microscope (Olympus, Tokyo, Japan).

Immunofluorescence was carried out as previously described [19]. Briefly, samples were incubated with a mixture of primary antibodies including anti-rabbit TMEM26 (1:50, NBP2–27334; Novus Biologicals Europe, Abingdin, UK) and anti-goat UCP1 (1:75), SAB2501082) overnight at 4 °C after blocking 1 h with donkey and sheep serums, respectively. Then, sections were incubated 2 h at room temperature (RT) with anti-rabbit-fluorescein isothiocyanate (FITC, 1:50, F7512; Merk KGaA, Darmstadt, Germany) followed by 2 h incubation at RT with anti-goat-tetramethyl rhodamine isothiocyanate (FITC, 1:50, ab6522; Abcam, Oxford, UK). Next, 4´,6´-diamidino-2-phenylindole (DAPI) medium was added to visualize cell nuclei. For negative control, the slides were incubated with PBS plus 0.3% Triton X-100, 10% donkey serum (DS), and 10% sheep serum (SS) for 1 h and then, incubated overnight at 4 °C with PBS plus 5% donkey serum (DS), and 5% sheep serum (SS). Next, sections were incubated 2 h at room temperature (RT) with the secondary antibody, anti-rabbit-fluorescein isothiocyanate (FITC, 1:50, F7512; Merk KGaA, Darmstadt, Germany), followed by incubation during 2 h at RT with the secondary antibody, anti-goat-tetramethyl rhodamine isothiocyanate (FITC, 1:50, ab6522; Abcam, Oxford, UK). Finally, FluoroShield 4′,6-diamidino-2-phenylindole (DAPI) medium was added. All samples were photographed using an Olympus BX61 microscope. Fluorescence photomicrographs were captured with a digital camera (DP70; Olympus, Tokyo, Japan) and software DP Controller (1.2.1.108; Olympus, Tokyo, Japan). (20X).

2.10. Transmission electron microscopy (TEM)

In order to analyze ingWAT ultrastructure, and to confirm the presence of mitochondria in ingWAT of mice treated with miR-21 mimic, TEM was carried out following a standard protocol [23]. Briefly, the samples were fixed with 2.5% glutaraldehyde solution during 75 h and then washed in phosphate buffer. Next, the samples were incubated in a series of buffers, starting with phosphate buffer, osmium 2%, distilled water and finally graded acetone using Automatic Sample Processor (electron microscope [EM] TP; Leica, Nussloch, Germany). Then, the

sections were included in graded series of Epon resin followed by semithin cuts using a glass blade (300 nm). Finally, ultrathin cuts were performed in areas of interest, previously identified using toluidine blue staining (89640; Merck KGaA, Darmstadt, Germany). Ultrathin sections were collected on copper grids (300 mesh), examined by transmission microscope with a voltage of 80 kV (Libra-120; Zeiss, Oberkochen, Germany), and the images recorded using iTEM software (Olympus, Tokyo, Japan).

2.11. Statistical analysis

All values are expressed as the mean ± SEM. Student's *t*-test or non-parametric Mann-Whitney U-test were performed to make comparisons between two groups. Comparisons between multiple groups was carried out using one-way ANOVA followed by Bonferroni's Post Hoc test or Kruskal-Wallis non-parametric test followed by Dunns's Post Hoc test. Shapiro-Wilk test was used for normality distribution analysis. Cumulative body weight was analyzed by repeated measurements and two-way ANOVA. Statistical analysis and graphics were performed using IBM SPSS statistics 22 and GraphPad Prism 5.00.288. Values $p<0.05$ was considered significant.

3. Results

3.1. Synthesis of high-quality, monodispersed, positively charged, and stabilized gold nanoparticles (Au@16-ph-16/miR-21 mimic) for efficient miR-21 mimic delivery

We have developed a novel nanosystem combining gold nanoparticles with the gemini surfactant as a delivery vehicle for miRNAs. Our tests show this system can efficiently compress miRNAs, exhibits excellent stability, and good cell-entry properties (Fig. 1A). We synthesized gold nanoparticles with a positive surface charge, Au@ 16-ph-16/miR-21 mimic, following our previously described method [33]. The synthesis approach uses hydrogen tetrachloroaurate, sodium tetrahydroborate, and 16-ph-16 compounds as gold precursor, reducing agent, and stabilizers, respectively. Nanoparticles obtained with this method were then coated with the miR-21 mimic polymer (Fig. 1A). As previously reported, the 16-ph-16 surfactant confers a lipophilic characteristic to the Au@16-ph-16/miR-21 mimic nanosystem [33].

3.2. In vivo treatment with Au@16-ph-16/miR-21 mimic nanosystem effectively inhibited weight gain and increased miR-21 levels in adipose tissues, in HFD-induced obese mice

Diet-induced obese mice were obtained after 8-week HFD feeding containing 45% of Kcal from saturated fat (45% HFD). After 8 weeks of feeding, obese mice were separated into three subgroups and subcutaneously injected for a further 6 weeks with 1) Au@16-ph-16, 2) 0.2 μg of Au@16-ph-16/miR-21 mimic and 3) 0.3 μg of Au@ 16-ph-16/miR-21 mimic and fed 45% HFD. Au@16-ph-16 at $8.5{\cdot}10^{-8}$ M concentration. (Fig. 1B).

Fig. 2A shows that Au@16-ph-16/miR-21 mimic at both concentrations (0.2 μg and 0.3 μg) significantly slowed body weight gain compared with control treatment (Au@16-ph-16). As illustrated in cumulative weight gain and weight AUC graphs, the administration of miR-21 mimic maintained and stabilized animal weight, while control mice continued to gain weight.

However, despite a noticeable trend towards improved glucose tolerance with Au@16-ph-16/miR-21 mimic treatment at both 0.2 and 0.3 μg compared to the control (Fig. S1), the results did not reach statistical significance. Therefore, we cannot conclude that the treatment was effective in increasing glucose tolerance. Moreover, no changes were observed in the normal fur, behavior, activity, or weight of the mice with this treatment. Moreover, there were no signs of depression or palpable nodules detected. Additionally, no mice died before the completion of the study.

To ascertain whether *in vivo* treatment with Au@16-ph-16/miR-21 mimic increased miR-21 expression levels in adipose and non-adipose tissues, the expression levels of miR-21 were analyzed. Fig. 2B shows that the expression of miR-21 was significantly increased in VAT, ingWAT and BAT in mice treated with Au@16-ph-16/miR-21 mimic versus control. Despite an upward trend in plasma miR-21 levels, no significant changes were observed (Fig. 2B). Furthermore, examination of miR-21 expression levels in non-adipose tissues, including the heart, liver, spleen, kidney, and brain, revealed no significant changes in the levels of this miRNA following the treatment (Fig. S2).

3.3. The in vivo treatment with Au@16-ph-16/miR-21 mimic nanosystem induced the expression of browning and thermogenesis genes in WAT and BAT

To investigate whether the effect of Au@16-ph-16/miR-21 mimic treatment on body weight was associated with thermogenesis and browning, we analyzed the expression levels of target genes, mainly those involved in the signaling pathways by which miR-21 could act in the activation of thermogenesis and browning of WAT of mice, as we have previously described [19], in both BAT and WAT from treated mice. As shown in Fig. 3, compared to control treatment with Au@16-ph-16, the treatment with Au@ 16-ph-16/miR-21 mimic at doses of 0.2 μg and 0.3 μg induced significantly increased expression of *Ucp1, Tmem26, Prdm16*, *Pgc-1α*, *Fgf21*, *Pparγ* in ingWAT; significantly increased expression of *Ucp1, Tmem26, Pgc-1α*, and *Vegf-A and Fgf21* in intWAT, and significantly increased expression of *Ucp1, Vegf-A, Prdm16, Pgc-1α* and *Cidea* in BAT. On the other hand, *p53* and *Tgfβ1*, which are two validated target genes of miR-21 described to regulate the beige cell formation and inhibit thermogenesis [19], were downregulated in ingWAT, intWAT and BAT. We might expect that the induction of browning and blocking of weight gain would be associated with changes in adipose tissue weights. Fig. S3 shows that VAT, intWAT, and ingWAT from mice treated with Au@16-ph-16/miR-21 mimic displayed lower weights compared to the control group, but this difference was not statistically significant.

3.4. The in vivo treatment with Au@16-ph-16/miR-21 mimic nanosystem induced the appearance of a brown-like adipocyte phenotype in WAT

Hematoxylin-eosin staining showed that the *in vivo* treatment with Au@16-ph-16/miR-21 mimic induced a brown-like adipocyte phenotype in both ingWAT and intWAT, characterized by small size and the presence of numerous lipid droplets, while the ingWAT and intWAT from control Au@16-ph-16 treated mice were primarily composed of unilocular adipocytes. In BAT, hematoxylin-eosin staining revealed the presence of multilocular adipocytes in both Au@16-ph-16/miR-21 mimic (0.2 μg) and control-treated groups (Fig. 4). Additionally, immunofluorescence staining showed that the intWAT and ingWAT from Au@16-ph-16/miR-21 mimic (0.2 μg) treated mice exhibited higher UCP1 and TMEM26 protein expression compared to the control Au@ 16-ph-16. Co-expression of both TMEM26 and UCP1 was detected in both ingWAT and intWAT from Au@16-ph-16/miR-21 mimic-treated mice (merged image) (Fig. 4A). BAT from Au@16-ph-16/miR-21 mimic (0.2 μg) treated mice exhibited higher levels of UCP1 compared to the control, while no signal corresponding to TMEM26 was detected (Fig. 4A). In contrast, VAT from control Au@16-ph-16 and Au@16-ph-16/miR-21 mimic (0.2 μg) treated mice were primarily composed of unilocular adipocytes (Fig. S4). Moreover, no immunofluorescence staining corresponding to TMEM26 and UCP1 was detected in VAT (Fig. S4).

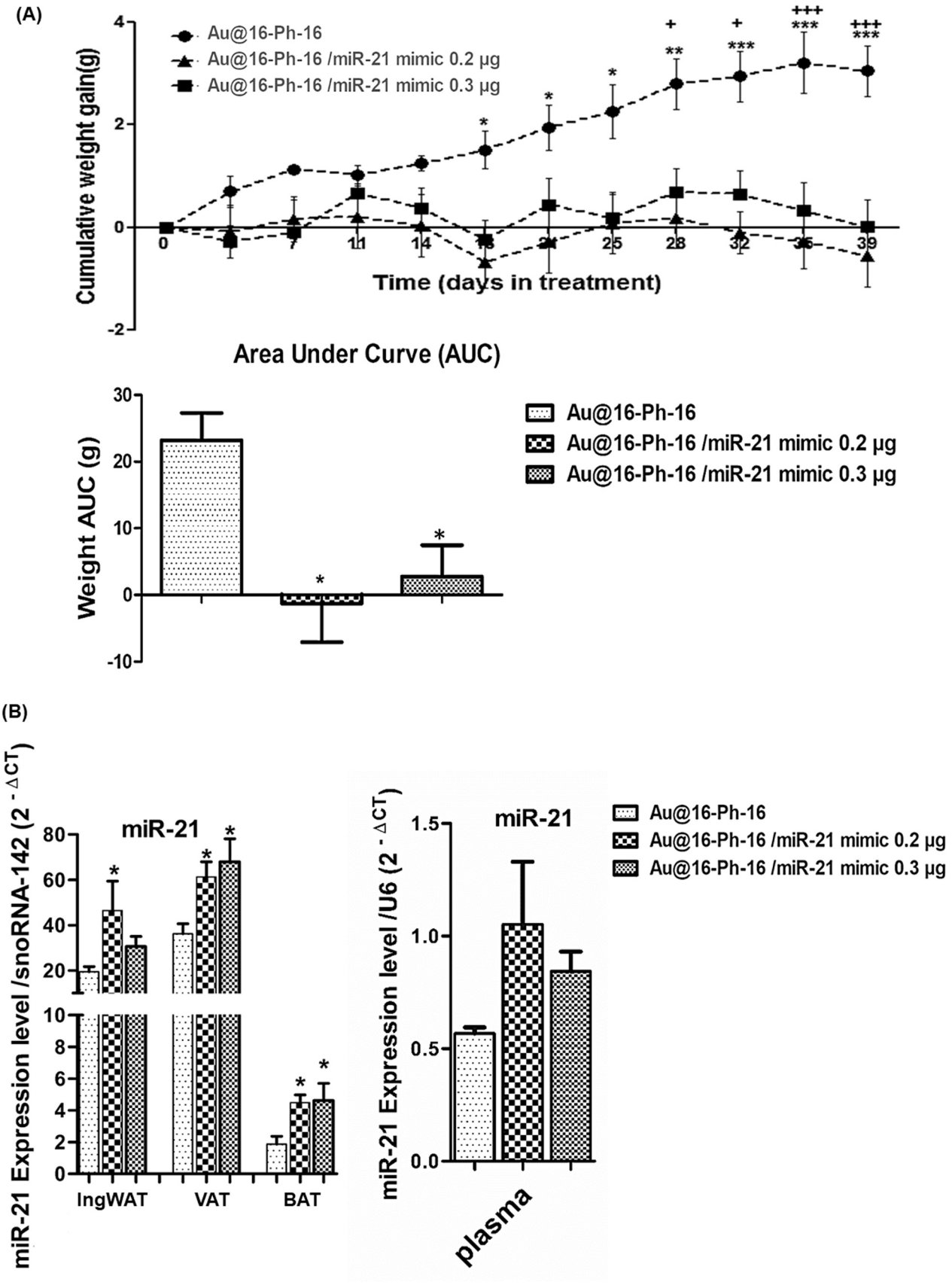

(caption on next page)

Fig. 2. The *in vivo* effects of Au@ 16-ph-16/miR-21 mimic treatment on weight gain and miR-21 expression in C57BL/6 J HFD obese mice. Obese C57BL/6 J mice fed 45% HFD during 8 weeks were injected subcutaneously with 0.2 μg (n = 9), 0.3 μg (n = 9) Au@ 16-ph-16/miR-21 mimic or control Au@ 16-ph-16 (n = 5) twice a week for 6 weeks. (A) Body weight was monitored twice a week during the 14 weeks. Cumulative weight and AUC were calculated using the weight before the start of the treatment as the basal point (0). (B) miR-21 expression levels were measured by real-time qPCR in inguinal white adipose tissue (ingWAT), BAT, VAT and plasma from treated mice using snoRNA-142 (in AT) or U6 (in plasma) as reference gene ($2^{-\Delta ct}$). Data are expressed as the mean ± SEM. *p<0.05, * **p<0.001 0.2 μg Au@ 16-ph-16/miR-21 mimic versus control, +p < 0.05 and + ++p < 0.001 0.3 μg Au@ 16-ph-16/miR-21 mimic versus control. Repeated ANOVA measurements, one-way ANOVA with Bonferroniś posthoc test or Kruskal-Wallis nonparametric test with Dunnśs posthoc test were used for statistical analysis. Shapiro-wilk was used to test the normality. Kruskal-Wallis nonparametric test was carried out in ingWAT.

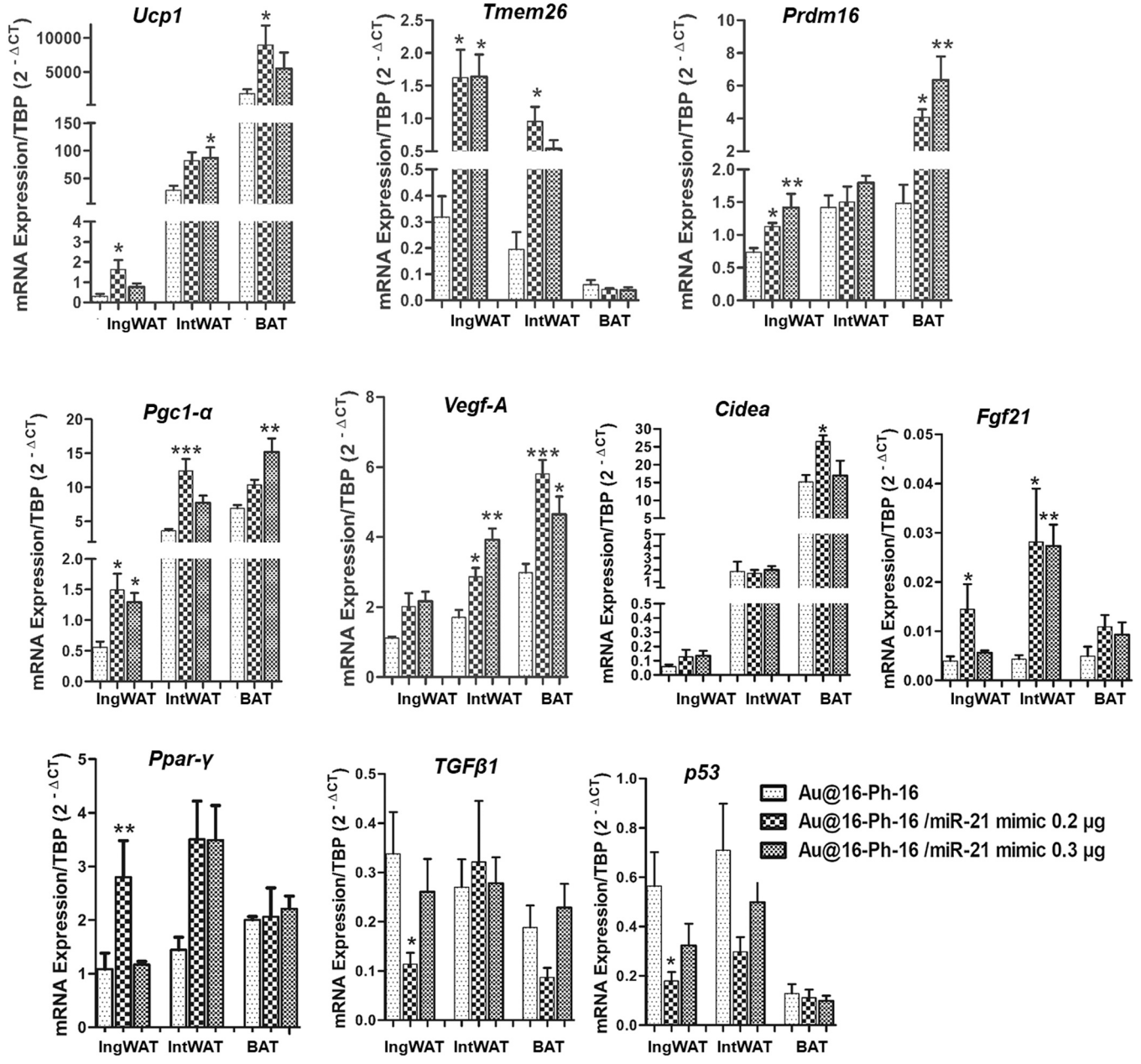

Fig. 3. The *in vivo* effect of Au@16-ph-16/miR-21 mimic treatment on the mRNA expression of browning and thermogenesis markers in WAT and BAT. The mRNA expression levels of thermoregulatory and browning markers were measured by real-time qPCR using TATA sequence binding protein (*Tbp*) as a reference gene ($2^{-\Delta ct}$) in ingWAT, intWAT and BAT from treated mice with 0.2 μg (n = 7) or 0.3 μg (n = 7). Au@16-ph-16/miR-21 mimic and Au@16-ph-16 control (n = 5). Data are expressed as the mean ± SEM. *p<0.05, * *p<0.01 and ***p<0.001 versus Au@16-ph-16 control according to one-way ANOVA with Bonferroniś posthoc test or Kruskal-Wallis nonparametric test with Dunnśs posthoc. Shapiro-wilk was used to test the normality. Kruskal-Wallis nonparametric test was carried out in BAT: *Ucp1, Prdm16, P53* and *Fgf21*; IngWAT: *Tmem26*, *Pparγ* and *Fgf21*; IntWAT: *Fgf21*.

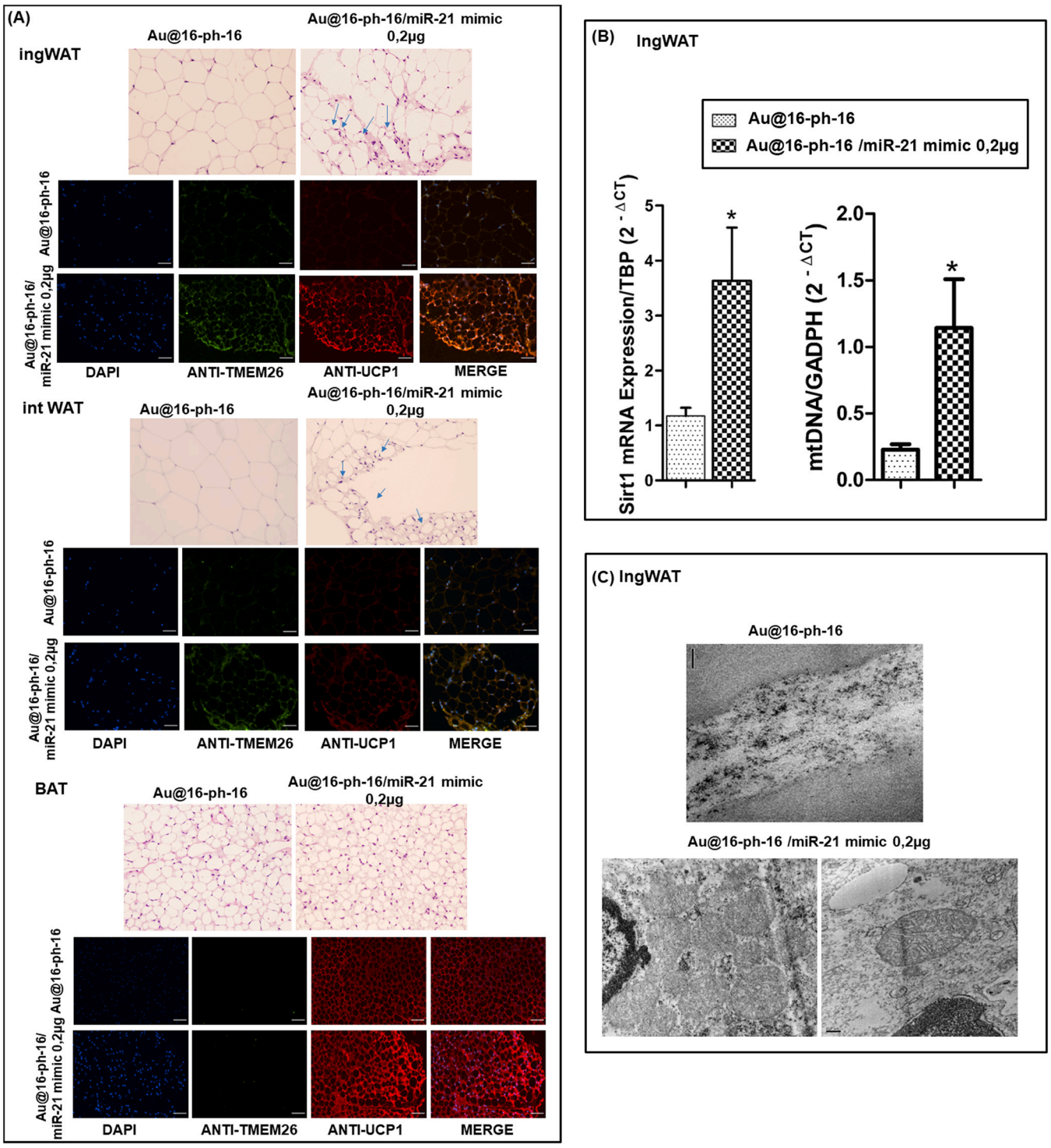

Fig. 4. Histological and mitochondria content analysis of WAT and BAT. Upon the completion of *in vivo* treatment with 0,2 µg Au@16-ph-16/miR-21 mimic or control, **(A)** paraffin sections of inguinal white adipose tissue (ingWAT), interscapular white adipose tissue (intWAT) and brown adipose tissue (BAT) were stained by hematoxylin and eosin (X20) or immunostained with rabbit anti-TMEM26 (green), goat anti-UCP1 (red), and nuclei stained with DAPI (blue). Images were visualized by fluorescence microscopy (X20, n = 3). Scale bars, 50 µm. (B) *Sirt1* mRNA expression was measured by real-time qPCR using TATA sequence binding protein (*Tbp*) as a reference gene ($2^{-\Delta ct}$) from the inguinal white adipose tissue (ingWAT) of mice treated with 0.2 µg Au@16-ph-16/miR-21 mimic (n = 7) or control (n = 5). COX1 as mitochondrial target and GAPDH as nuclear target were measured from ingWAT by real-time qPCR. Relative mtDNA content was calculated using the formula: mtDNA= $2^{-\Delta ct}$, where ΔCt= $_{Ct}$ COX1 - $_{Ct}$ GADPH. **(C)** Adipocytes ultrastructure was analyzed by transmission electron microscopy (TEM) from ingWAT of mice treated with 0,2 µg Au@ 16-ph-16/miR-21 mimic or control. Scale bars, 0.5 µm. Data are expressed as the mean ± SEM. *p<0.05 versus Au@16-ph-16 control. Student's t-test was used for statistical analysis. Shapiro-wilk was used to test the normality. The expression of Sirt1 and mtDNA was normally distributed.

3.5. In vivo Au@16-ph-16/miR-21 mimic treatment increased Sirt1 expression, the appearance of mitochondria, and mitochondrial DNA content in ingWAT

Sirt1 gene expression, ultrastructure analysis by TEM and mitochondrial DNA content analysis were carried out in ingWAT, to ensure that the effect of Au@16-ph-16/miR-21 mimic on browning and thermogenesis induction was accompanied by mitochondrial biogenesis. Fig. 4B shows that treatment with Au@16-ph-16/miR-21 mimic 0.2 μg significantly increased the copy number of mtDNA in ingWAT compared with Au@16-ph-16 control. Moreover, the expression of *Sirt1*, which is known to play a crucial role in mitochondrial biogenesis by PGC-1α deacetylation [39,40], increased in ingWAT from mice treated with Au@16-ph-16/miR-21 mimic 0.2 μg versus the Au@16-ph-16 control. Furthermore, large and abundant mitochondria were much more frequent in Au@16-ph-16/miR-21 mimic-treated mice than in samples from the Au@16-ph-16 control (Fig. 4C).

4. Discussion

Managing obesity is a challenging task in clinical practice, as current therapeutic options often yield limited and non-sustained results. Despite significant progress in understanding this condition, current knowledge falls short in effectively addressing this epidemic. Consequently, there is an urgent need to explore new therapies to prevent and treat obesity.

This study provides compelling evidence that the miR21 mimic, encapsulated within the Au@16-ph-16 delivery system, effectively sustained its effects on weight gain and browning induction. In fact, the Au@16-ph-16/miR21 mimic nanosystem induced a significant 7% reduction in weight gain associated with browning and thermogenesis. Moreover, this nanocarrier enabled to obtain an effect with the synthetic miR-21 mimic at a dose of 0.2 μg, significantly lower than the doses typically utilized with polyethylenimine carrier (JetPEI) (0,5, 20 and 40 μg) [19,41,42]. Additionally, it enabled the development of a delivery system with a significantly smaller structural size, ranging from 10 to 13 nm, in contrast to the JetPEI polymer, which has a much larger size often exceeding hundreds of nanometers.

Changing the carrier used for synthetic miRNA delivery, could potentially alter the signaling pathways triggered by the miRNA, therefore it is important to verify the functionality of the new method. Significantly, the results obtained with the Au@ 16-ph-16 carrier, are broadly in line with our previous study where a synthetic miR-21 mimic was delivered with JetPEI [19]. We found that encapsulation and delivery with the Au@ −16-ph-16 carrier does not affect the ability of the miR-21 mimic to regulate browning and thermogenesis, or modulate VEGF-A, p53, and TGFβ1 signaling pathways, specifically through the regulation of genes involved in these pathways including *Vegf-A*, *Tmem26, Pgc-1α, Prdm16, Cidea, Ppar-γ, P53, Tgf-β1, Fgf21,* and *Sirt1*.

Although similar results have been obtained with JetPEI, and no adverse effects have been observed in the animal model used in the previous study [19], the use of JetPEI requires the inclusion of a 10% isotonic glucose solution to form small and stable nucleic acid/*in vivo*-jetPEI® complexes [19]. This limitation makes JetPEI an inappropriate choice as a carrier for future clinical trials involving humans obese, especially subjects with type 2 diabetes. Moreover, effective therapeutic delivery systems should possess the capability to precisely target specific tissues or cells while minimizing off-target effects. In our case, the main challenge lies in delivering the miR-21 mimic specifically to AT. Unlike certain tissues or organs that have distinctive cell surface proteins that can be targeted, AT lacks such specific markers due to its diverse cellular composition, including adipocytes, a complex network of blood vessels, extracellular matrix, and other cell types [43]. This complexity makes it challenging to design targeting strategies that exclusively and efficiently deliver drugs to AT while avoiding off-target effects in other tissues. The JetPEI carrier lacks selective specificity for AT, which may result in delivery to non-adipose tissues [46 [41,42,44]. To overcome these challenges, we have joined other researchers in exploring alternative targeting strategies, such as nanoparticles with specific properties that can enhance accumulation in adipose tissue and achieve selective drug delivery [31]. In this regard, previous approaches for delivering miRNAs using gold nanoparticles have often faced challenges due to the complex procedures required to attach miRNA to the gold nanoparticles [34]. However, in this study, we present a novel and comparatively straightforward method for producing monodisperse Au@16-ph-16/miR-21 nanoparticles, offering an easy and efficient approach. Au@16-ph-16/miR-21 includes cationic gemini 16-ph-16 surfactants, which are amphiphilic compounds with excellent hydrophilic-hydrophobic balance (HLB) values, making them suitable for various applications such as detergents, pharmacy, or personal care products [36,37]. According to Davies' method, the HLB value for the 16-Ph-16 gemini surfactant is 6.1, categorizing it as a lipophilic molecule [45]. Therefore, we propose that the lipophilic nature of the Au@16-ph-16/miR-21 mimic nanosystem may result in increased interaction with AT compared to non-adipose organs. This potential specificity holds promise for minimizing off-target effects and toxicity [43]. To strengthen our hypothesis, in a comparative study between JetPEI and Au@16-ph-16 as two distinct carriers for the miR21 mimic, it was observed that when the miR21 mimic was delivered with the Au@16-ph-16 nanosystem as a vehicle, it did not reach other tissues, such as the heart, liver, spleen, brain, and kidney. This observation was based on the absence of significant increases in miR21 levels detected in these organs after the *in vivo* treatment (Fig. S3). In contrast, when using JetPEI, substantial increases in miR21 levels, especially in the heart, liver, and kidney, were observed after treatment (Fig. S5). This finding suggests that designing a therapy specifically tailored to target AT might be more effective and straightforward using Au@16-ph-16 compared to JetPEI. However, it should be acknowledged that these lipophilic characteristics may also allow the nanosystem to reach other organs where, also, fat accumulates, such as the heart or liver. Thus, further studies and technologies should be conducted to guarantee that the delivery of this nanosystem is exclusively limited to AT. For this therapy, we believe that subcutaneous fat would be the most appropriate target tissue, as its local application would be less bothersome and invasive for the patient compared to visceral fat. Application to visceral fat, for example, would require a more invasive and painful technology.

In this study, although we observed an increase in miR-21 levels in visceral fat, we were unable to detect browning induction in this tissue. This was expected, as it is known that in mice, visceral fat is less susceptible to browning, while in humans, the pattern is different, and visceral fat is more prone to browning than subcutaneous fat [46]. Despite this, visceral fat remains an unfavorable candidate as a target tissue for this type of therapy due to the requirement for more invasive protocols for the patient.

In terms of future perspectives, despite the lipophilic surfactant present in this nanosystem, further studies and technologies should be conducted to ensure that the delivery of this nanosystem is exclusively limited to AT. Additionally, we are convinced that the strong positive charge of the Au@16-ph-16/miR-21 mimic nanosystem, along with its size and form, can be harnessed to effectively confine the presence of the miR-21 mimic to the localized site of administration, thereby reducing any unintended dispersion.

It is important to highlight that, in addition to ensuring the specific delivery of the nanosystem to AT, it is also necessary to ensure that traces of Au@ nanoparticles do not remain in certain organs. In this regard, in our previous study of Au@16-ph-16/miR-21 mimic toxicity we obtained encouraging results [33] as ex-vivo CARS microscopy experiments provided evidence of the non-accumulation of these Au@ nanoparticles in the principal organs studied, including livers, spleens, lungs, brains, kidneys, and fat tissue. However, additional studies are needed in order to verify the safety of this approach.

Another point to emphasize is, anticipation of future clinical trials,

the utilization of a minimal quantity of miRNA mimic may be imperative, as it would allow for a meticulous and controlled assessment of the therapy's potential benefits while mitigating potential risks and improving cost-effectiveness. Typically, achieving a successful therapeutic effect with synthetic miRNA requires higher amounts compared to those used in our nanosystem [47]. Here, the use of lower quantities of miR-21 mimic in our nanosystem when compared to the JetPEI system led to minimize non-specific side effects or accumulation in other tissues, which would be beneficial during prolonged treatment, while also improving cost-effectiveness.

Moreover, to date previous attempts to enhance therapeutic effects by improving the interaction between AT and nanoparticles have required complex engineering and the incorporation of functional molecules, such as targeting ligands, resulting in larger nanostructures [48]. Our nanosystem overcomes this limitation by utilizing a smaller gold core (~3 nm) and a non-complex structure (diameter of 10–13 nm) [33], which may allow increasing drug loading capacity, enabling the delivery of larger quantities of therapeutic agents, improving cellular uptake and reduce the risk of toxicity, and thereby minimizing potential adverse effects [46]. Recent studies describe potential nanotechnology-based treatments, where nanoparticles are coated with peptides to target WAT, such as Rosiglitazone, an agonist of the peroxisome proliferator-activated receptor γ (PPARγ) [49], and the Notch inhibitor, Dibenzazepine (DBZ) [50]. To minimize the off-target effects of Rosiglitazone and maximize its browning activity, required complex engineering of the delivery system, where Rosi is encapsulated into prohibitin-targeted nanoparticles, modified with an octaarginine peptide ligand via a long prostaglandin E2 analog linker to enhance cell penetration and uptake, resulting in a large nanosystem with a diameter of 90–100 nm [49]. In other studies, researchers have used localized delivery into adipose tissue, such as injecting DBZ-loaded NPs (with a size of 177 nm) into the inguinal WAT deposits of diet-induced obese mice, which resulted in adipocyte browning, improved glucose homeostasis, and reduced body weight gain of the treated mice [50].

This study has also other limitations. We used miR-21 expression as a readout for miR-21 delivery and could not distinguish between endogenous and exogenous miR-21. Hence, we cannot discard that the nanosystem is somehow increasing miR-21 expression, together with being specifically delivered to the adipose tissue. Further studies tracing either the nanosystem itself or the exogenous miR-21 are warranted.

5. Conclusions

The data presented in this study underscores the promising potential of Au@ 16-ph-16/miR-21 mimic as a therapeutic solution for obesity and its related conditions in the realm of clinical translation. Altogether, the current findings, along with our prior research [19,33], significantly contribute to advancing the Technology Readiness Levels. This progress opens up a pathway for future investigations and the initiation of clinical trials and human studies to assess the efficacy and safety of the Au@ 16-ph-16/miR-21 mimic nanosystem in individuals dealing with obesity and metabolic disorders.

Funding

This research was supported by the following grants: This study has been funded by Instituto de Salud Carlos III (ISCIII) through the project PI21/01924 and PI18/00785 and co-funded by the European Union, by the Consejería de Transformación Económica, Industria, Conocimiento y Universidades-Junta de Andalucía and ERDF-EU (PI20-01274) and by University of Sevilla VI PP USO SSGG (2021/00001297). PI-0092–2017 and PI-0235–2021 from Consejeria de Salud (Junta de Andalucia), Spain. S.L. is a recipient of a Plan Andaluz de Investigación, Desarrollo e Innovación post-doctoral grant from the Consejería de Economía, Conocimiento, Empresas y Universidades (DOC-01138). A.M.G. was a recipient of a Plan Propio de Investigación, Transferencia y Divulgación Científica postdoctoral grant from University of Málaga. FJBS, and REBAV-R are under contract with the 'Nicolas Monardes' program from the Servicio Andaluz de Salud, Consejería de Salud y Consumo-Junta de Andalucía (RC-0001-2021, RC-0006-2020 and C-0060-2018, respectively. A.V-R. was supported by a grant from the Ministerio de Economía y Competitividad (Proyectos I+D+i para Jóvenes Investigadores, SAF2014-60649-JIN)

CRediT authorship contribution statement

Mengual-Mesa Maria: Conceptualization, Data curation, Formal analysis, Investigation, Methodology. **Gentile Adriana-Mariel:** Data curation, Formal analysis, Investigation, Methodology. **Giráldez-P é rez Rosa M:** Investigation, Methodology. **Grueso Elia:** Investigation, Methodology. **Bermudez-Silva Francisco-Javier:** Methodology. **Olveira Gabriel:** Methodology. **Lhamyani Said:** Conceptualization, Data curation, Formal analysis, Investigation, Methodology, Writing – review & editing. **Vega-Rioja Antonio:** Methodology. **El Bekay Rajaa:** Conceptualization, Data curation, Formal analysis, Funding acquisition, Investigation, Project administration, Resources, Supervision, Validation, Writing – original draft, Writing – review & editing. **Fernandez-Garcia José Carlos:** Methodology. **González-Mariscal Isabel:** Methodology. **Pearson John R:** Methodology. **Clemente-Postigo Mercedes:** Methodology.

Declaration of Competing Interest

The authors have no conflicts of interests to declare.

Data Availability

Data will be made available on request.

Acknowledgements

The Centro de Investigación Biomédica en Red de Fisiopatología de la Obesidad y Nutrición (CIBERobn), Centro de Investigación Biomédica en Red de Diabetes y Enfermedades Metabólicas Asociadas. (CIBERdem) and Centro de Investigación Biomédica en Red de las Enfermedades Cardiovasculares (CIBERCV) are part of the Instituto de Salud del Carlos III (ISCIII). The authors are grateful to the Microscopy and Functional Characterization Service of the Research, Technology and Innovation Center of the University of Seville (CITIUS).

Appendix A. Supporting information

Supplementary data associated with this article can be found in the online version at doi:10.1016/j.biopha.2023.116104.

References

[1] V.A. Eley, M. Thuzar, S. Navarro, B.R. Dodd, A.A. van Zundert, Obesity, metabolic syndrome, and inflammation: An update for anaesthetists caring for patients with obesity, Anaesth. Crit. Care Pain. Med. vol. 40 (6) (. 2021), https://doi.org/10.1016/J.ACCPM.2021.100947.

[2] A. Engin, The definition and prevalence of obesity and metabolic syndrome, Adv. Exp. Med Biol. vol. 960 (2017) 1–17, https://doi.org/10.1007/978-3-319-48382-5_1.

[3] V. Shettar, S. Patel, S. Kidambi, Epidemiology of obesity and pharmacologic treatment options, Nutr. Clin. Pr. vol. 32 (4) (. 2017) 441–462, https://doi.org/10.1177/0884533617713189.

[4] A. Hruby, F.B. Hu, The epidemiology of obesity: a big picture, Pharmacoeconomics vol. 33 (7) (. 2015) 673–689, https://doi.org/10.1007/S40273-014-0243-X.

[5] M.O. Dietrich, T.L. Horvath, Limitations in anti-obesity drug development: the critical role of hunger-promoting neurons, Nat. Rev. Drug Discov. vol. 11 (9) (. 2012) 675–691, https://doi.org/10.1038/NRD3739.

[6] L. Sidossis, S. Kajimura, Brown and beige fat in humans: thermogenic adipocytes that control energy and glucose homeostasis, J. Clin. Investig. vol. 125 (2) (. 2015) 478–486, https://doi.org/10.1172/JCI78362.

[7] A.M. Cypess, et al., Identification and importance of brown adipose tissue in adult humans, N. Engl. J. Med. vol. 360 (15) (. 2009) 1509–1517, https://doi.org/10.1056/NEJMOA0810780.
[8] K.A. Lo, L. Sun, Turning WAT into BAT: a review on regulators controlling the browning of white adipocytes, Biosci. Rep. vol. 33 (5) (2013) 711–719, https://doi.org/10.1042/BSR20130046.
[9] A.L. Poher, J. Altirriba, C. Veyrat-Durebex, F. Rohner-Jeanrenaud, Brown adipose tissue activity as a target for the treatment of obesity/insulin resistance, Front. Physiol. vol. 6 (JAN) (2015), https://doi.org/10.3389/FPHYS.2015.00004.
[10] M. Harms, P. Seale, Brown and beige fat: development, function and therapeutic potential, Nat. Med. vol. 19 (10) (. 2013) 1252–1263, https://doi.org/10.1038/NM.3361.
[11] A. Kuryłowicz, M. Puzianowska-Kuźnicka, Induction of adipose tissue browning as a strategy to combat obesity, Int. J. Mol. Sci. vol. 21 (17) (2020) 1–28, https://doi.org/10.3390/IJMS21176241.
[12] S.H. Kim, J. Plutzky, Brown fat and browning for the treatment of obesity and related metabolic disorders, Diabetes Metab. J. vol. 40 (1) (2016) 12–21, https://doi.org/10.4093/DMJ.2016.40.1.12.
[13] J. Wu, P. Cohen, B.M. Spiegelman, Adaptive thermogenesis in adipocytes: is beige the new brown? Genes Dev. vol. 27 (3) (. 2013) 234–250, https://doi.org/10.1101/GAD.211649.112.
[14] P. Seale, et al., Prdm16 determines the thermogenic program of subcutaneous white adipose tissue in mice, J. Clin. Invest vol. 121 (1) (. 2011) 96–105, https://doi.org/10.1172/JCI44271.
[15] J.A. Slota, S.A. Booth, MicroRNAs in neuroinflammation: implications in disease pathogenesis, biomarker discovery and therapeutic applications, Noncoding RNA vol. 5 (2) (. 2019), https://doi.org/10.3390/NCRNA5020035.
[16] H. Zhong, M. Ma, T. Liang, L. Guo, Role of MicroRNAs in obesity-induced metabolic disorder and immune response, J. Immunol. Res. vol. 2018 (2018), https://doi.org/10.1155/2018/2835761.
[17] A. Vishnoi, S. Rani, miRNA biogenesis and regulation of diseases: an updated overview, Methods Mol. Biol. vol. 2595 (2023) 1–12, https://doi.org/10.1007/978-1-0716-2823-2_1.
[18] M. Karbiener, M. Scheideler, MicroRNA functions in brite/brown fat - novel perspectives towards anti-obesity strategies, Comput. Struct. Biotechnol. J. vol. 11 (19) (. 2014) 101–105, https://doi.org/10.1016/J.CSBJ.2014.09.005.
[19] S. Lhamyani, et al., miR-21 mimic blocks obesity in mice: a novel therapeutic option, Mol. Ther. Nucleic Acids vol. 26 (. 2021) 401–416, https://doi.org/10.1016/J.OMTN.2021.06.019.
[20] A.M. Gentile, et al., miR-20b, miR-296, and Let-7f expression in human adipose tissue is related to obesity and type 2 diabetes, Obes. (Silver Spring) vol. 27 (2) (. 2019) 245–254, https://doi.org/10.1002/OBY.22363.
[21] J. Sánchez-Ceinos, et al., miR-223-3p as a potential biomarker and player for adipose tissue dysfunction preceding type 2 diabetes onset, Mol. Ther. Nucleic Acids vol. 23 (. 2021) 1035–1052, https://doi.org/10.1016/J.OMTN.2021.01.014.
[22] T. Seeger, A. Fischer, M. Muhly-Reinholz, A.M. Zeiher, S. Dimmeler, Long-term inhibition of miR-21 leads to reduction of obesity in db/db mice, Obes. (Silver Spring) vol. 22 (11) (. 2014) 2352–2360, https://doi.org/10.1002/OBY.20852.
[23] Y. Mei, et al., miR-21 modulates the ERK-MAPK signaling pathway by regulating SPRY2 expression during human mesenchymal stem cell differentiation, J. Cell Biochem vol. 114 (6) (. 2013) 1374–1384, https://doi.org/10.1002/JCB.24479.
[24] D. Sekar, V.I. Hairul Islam, K. Thirugnanasambantham, S. Saravanan, Relevance of miR-21 in HIV and non-HIV-related lymphomas, Tumour Biol. vol. 35 (9) (. 2014) 8387–8393, https://doi.org/10.1007/S13277-014-2068-9.
[25] E. Jayawardena, L. Medzikovic, G. Ruffenach, M. Eghbali, Role of miRNA-1 and miRNA-21 in acute myocardial ischemia-reperfusion injury and their potential as therapeutic strategy, Int. J. Mol. Sci. vol. 23 (3) (. 2022), https://doi.org/10.3390/IJMS23031512.
[26] Y.Jeong Kim, S.Jin Hwang, Y.Chan Bae, J.Sup Jung, MiR-21 regulates adipogenic differentiation through the modulation of TGF-beta signaling in mesenchymal stem cells derived from human adipose tissue, Stem Cells vol. 27 (12) (. 2009) 3093–3102, https://doi.org/10.1002/STEM.235.
[27] H. Mollaei, R. Safaralizadeh, Z. Rostami, MicroRNA replacement therapy in cancer, J. Cell Physiol. vol. 234 (8) (. 2019) 12369–12384, https://doi.org/10.1002/JCP.28058.
[28] R. Liu, R. Zuo, G.A. Hudalla, Harnessing molecular recognition for localized drug delivery, Adv. Drug Deliv. Rev. 170 (2021) 238–260, https://doi.org/10.1016/j.addr.2021.01.008. Epub 2021 Jan 20. PMID: 33484737; PMCID: PMC8274479.
[29] B. Tu, M. Zhang, T. Liu, Y. Huang, Nanotechnology-based histone deacetylase inhibitors for cancer therapy, Front. Cell Dev. Biol. vol. 8 (. 2020), https://doi.org/10.3389/FCELL.2020.00400.
[30] S. Bayda, et al., Inorganic nanoparticles for cancer therapy: a transition from lab to clinic, Curr. Med. Chem. vol. 25 (34) (. 2018) 4269–4303, https://doi.org/10.2174/0929867325666171229141156.
[31] N. Thovhogi, N. Sibuyi, M. Meyer, et al., Targeted delivery using peptide-functionalised gold nanoparticles to white adipose tissues of obese rats, J. Nanopart. Res. 17 (2015) 112, https://doi.org/10.1007/s11051-015-2904-x.
[32] R.M. Tripathi, A. Shrivastav, B.R. Shrivastav, Biogenic gold nanoparticles: As a potential candidate for brain tumor directed drug delivery, Artif. Cells Nanomed. Biotechnol. 43 (5) (2015) 311–317, https://doi.org/10.3109/21691401.2014.885445.
[33] R.M. Giráldez-Pérez, et al., miR-21/Gemini surfactant-capped gold nanoparticles as potential therapeutic complexes: Synthesis, characterization and in vivo nanotoxicity probes, J. Mol. Liq. vol. 313 (. 2020) 113577, https://doi.org/10.1016/J.MOLLIQ.2020.113577.
[34] S.W.L. Lee, et al., MicroRNA delivery through nanoparticles, J. Control. Release vol. 313 (. 2019) 80–95, https://doi.org/10.1016/j.jconrel.2019.10.007.
[35] R. Ghosh, L.C. Singh, J.M. Shohet, P.H. Gunaratne, A gold nanoparticle platform for the delivery of functional microRNAs into cancer cells, Biomaterials vol. 34 (3) (. 2013) 807–816, https://doi.org/10.1016/J.BIOMATERIALS.2012.10.023.
[36] B. Brycki, A. Koziróg, I. Kowalczyk, T. Pospieszny, P. Materna, J. Marciniak, Synthesis, structure, surface and antimicrobial properties of new oligomeric quaternary ammonium salts with aromatic spacers, Molecules 22 (11) (2017 25) 1810, https://doi.org/10.3390/molecules22111810.
[37] D. Myers. Surfactant Science and Technology, Third ed., Wiley, Hoboken, NJ, USA; New York, NY, USA, 2006.
[38] A. Nolte, K. Ott, J. Rohayem, T. Walker, C. Schlensak, H.P. Wendel, Modification of small interfering RNAs to prevent off-target effects by the sense strand, N. Biotechnol. vol. 30 (2) (. 2013) 159–165, https://doi.org/10.1016/J.NBT.2012.10.001.
[39] B.L. Tang, Sirt1 and the mitochondria, Mol. Cells vol. 39 (2) (. 2016) 87–95, https://doi.org/10.14348/MOLCELLS.2016.2318.
[40] A. Nishigaki, H. Tsubokura, T. Tsuzuki-Nakao, H. Okada, Hypoxia: role of SIRT1 and the protective effect of resveratrol in ovarian function, Reprod. Med. Biol. vol. 21 (1) (. 2022) e12428, https://doi.org/10.1002/rmb2.12428.
[41] M. Giroud, M. Karbiener, D.F. Pisani, R.A. Ghandour, G.E. Beranger, T. Niemi, M. Taittonen, P. Nuutila, K.A. Virtanen, D. Langin, M. Scheideler, E.Z. Amri, Let-7i-5p represses brite adipocyte function in mice and humans, Sci. Rep. 6 (2016 27) 28613, https://doi.org/10.1038/srep28613. PMID: 27345691; PMCID: PMC4921928.
[42] J.H. Sohn, Y. Ji, C.Y. Cho, H. Nahmgoong, S. Lim, Y.G. Jeon, S.M. Han, J.S. Han, I. Park, H.W. Rhee, S. Kim, J.B. Kim, Spatial regulation of reactive oxygen species via G6PD in brown adipocytes supports thermogenic function, Diabetes 70 (12) (2021) 2756–2770, https://doi.org/10.2337/db21-0272. Epub 2021 Sep 14. PMID: 34521642.
[43] Y. Onogi, A.E.M.M. Khalil, S. Ussar, Identification and characterization of adipose surface epitopes, Biochem J. vol. 477 (13) (. 2020) 2509–2541, https://doi.org/10.1042/BCJ20190462.
[44] K. Schlosser, M. Taha, Y. Deng, D.J. Stewart, Systemic delivery of MicroRNA mimics with polyethylenimine elevates pulmonary microRNA levels, but lacks pulmonary selectivity, Pulm. Circ. vol. 8 (1) (. 2018), https://doi.org/10.1177/2045893217750613.
[45] R. Sowada, J.C. McGowan, Calculation of HLB Values / Berechnung von HLB-Werten einiger Struktureinheiten von Emulgatoren, Tenside Surfactants Deterg. vol. 29 (2) (1992) 109–113, https://doi.org/10.1515/tsd-1992-290208.
[46] R. Coradeghini, S. Gioria, C.P. García, P. Nativo, F. Franchini, D. Gilliland, J. Ponti, F. Rossi, Size-dependent toxicity and cell interaction mechanisms of gold nanoparticles on mouse fibroblasts, Toxicol. Lett. 217 (3) (2013 13) 205–216, https://doi.org/10.1016/j.toxlet.2012.11.022.
[47] Z. Sun, et al., In vivo multimodality imaging of miRNA-16 iron nanoparticle reversing drug resistance to chemotherapy in a mouse gastric cancer model, Nanoscale vol. 6 (23) (. 2014) 14343–14353, https://doi.org/10.1039/C4NR03003F.
[48] Y.H. Tsou, et al., Nanotechnology-mediated drug delivery for the treatment of obesity and its related comorbidities, Adv. Health Mater. vol. 8 (12) (. 2019), https://doi.org/10.1002/ADHM.201801184.
[49] R. Hiradate, I.A. Khalil, A. Matsuda, M. Sasaki, K. Hida, H. Harashima, A novel dual-targeted rosiglitazone-loaded nanoparticle for the prevention of diet-induced obesity via the browning of white adipose tissue, J. Control Release vol. 329 (. 2021) 665–675, https://doi.org/10.1016/J.JCONREL.2020.10.002.
[50] C. Jiang, et al., Dibenzazepine-loaded nanoparticles induce local browning of white adipose tissue to counteract obesity, Mol. Ther. vol. 25 (7) (. 2017) 1718–1729, https://doi.org/10.1016/J.YMTHE.2017.05.020.